Enhancing minority carrier lifetime in Ge: Insights from HF and HCl cleaning procedures

Alexandre Chapotot, Jérémie Chrétien, Oleh Fesiienko, Erwine Pargon, Jinyoun Cho, Kristof Dessein, Abderraouf Boucherif, Gwenaëlle Hamon, Maxime Darnon

Enhancing minority carrier lifetime in Ge: Insights from HF and HCl cleaning procedures

Running title: Enhancing minority carrier lifetime in Ge: Insights from HF and HCl cleaning procedures

Running Authors: Alexandre Chapotot[1,2,a], Jérémie Chrétien[1,2], Oleh Fesiienko[1,2,3], Erwine Pargon[3], Jinyoun Cho[4], Kristof Dessein[4], Abderraouf Boucherif[1,2], Gwenaëlle Hamon[1,2] and Maxime Darnon[1,2,a]

[1] Institut Interdisciplinaire d'Innovation Technologique (3IT), Université de Sherbrooke, 3000 Boulevard Université, Sherbrooke, J1K 0A5 Québec, Canada
[2] Laboratoire Nanotechnologies Nanosystèmes (LN2) - CNRS IRL-3463, Institut Interdisciplinaire d'Innovation Technologique (3IT), Université de Sherbrooke, 3000 Boulevard Université, Sherbrooke, J1K 0A5 Québec, Canada
[3] Univ. Grenoble Alpes, CNRS, CEA/LETI-Minatec, Grenoble INP, LTM, F-38054 Grenoble-France
[4] Umicore Electro-Optic Materials, Watertorenstraat 33, 2250, Olen, Belgium

[a)] Electronic mail: alexandre.chapotot@usherbrooke.ca / maxime.darnon@usherbrooke.ca

ABSTRACT

Efficiently passivating germanium (Ge) surfaces is crucial to reduce the unwanted recombination current in high-performance devices. Chemical surface cleaning is critical to remove surface contaminants and Ge oxides, ensuring effective surface passivation after dielectric deposition. However, Ge oxides can rapidly regrow upon air exposure. To understand the surface evolution after wet cleaning, we present a comprehensive study comparing HF and HCl deoxidation steps on p-type Ge surfaces and monitor the surface as a function of air exposure time. Distinct oxide regrowth dynamics are observed: HF-treated samples exhibit swift regrowth of all Ge oxide states, whereas HCl-treated Ge surfaces exhibit a lower concentration of low degrees of oxidation and slower or no regrowth of high oxide states even after 110 minutes of air exposure. In addition, the

presence of Ge-Cl bonds induces different oxidation dynamics compared to the Ge-OH bonds resulting from HF cleaning. This leads to varying surface electronic band structures, with HF-treated Ge exhibiting a strong positive band bending (+0.20 eV). Conversely, HCl-treated samples display a lower band curvature (+0.07 eV), mostly due to the presence of Ge-Cl bonds on the Ge surface. During air exposure, the increased GeO_x coverage significantly reduces the band bending after HF, while a constant band bending is observed after HCl. Finally, these factors induce a reduction in the surface recombination velocity (SRV) after wet etching. Combining both chemical and field-induced passivation, HF-treated Ge without rinsing exceeds 800 µs.

I. INTRODUCTION

Germanium (Ge) is used for many applications such as metal-oxide-semiconductor field-effect transistors (MOSFET) [1], free-standing membranes [2–5], IR lenses [6], biosensors [7], batteries [8], or multijunction solar cells [9]. In most cases, high-performance device fabrication requires a proper understanding and control of the Ge surface passivation. Indeed, the potential of Ge is hampered by its high surface defect density. These defects lead to a high charge carrier recombination rate at the surface and can compromise the channel's carrier mobility in MOSFET devices [10,11]. In optoelectronic devices, such as solar cells and lasers, the electronic states induced by surface defects can act as non-radiative recombination centers for minority charge carriers and therefore decrease the device's conversion efficiency [12]. To counteract this detrimental surface impact on the final device's performances, various passivation paths have been developed based on dielectric layer deposition [13–21]. Although many of these studies were more interested in determining and

optimizing the deposition parameters and the dielectric layers to obtain high passivation quality, some authors have mentioned the importance of the cleaning step performed prior to the deposition of the dielectric layer on the passivation performances [14,17]. Ge wafers are traditionally exposed to wet cleaning to etch the native Ge oxide and prevent oxide regrowth. However, unlike on silicon, the peroxide-based solution cannot be used with Ge due to their high etching rates [22]. From this observation, several cleaning techniques have been developed using water [23], ammonium hydroxide (NH_4OH) [24], thiols (-SH) [25], or organic compounds [26]. The cleaning step based on halogenated acid etchants (mostly HF and HCl) [27] has rapidly become widespread in the Ge industry by analogy with Si industrial cleaning steps.

Choi and Buriak [28] and Sun *et al.* [29] reported Ge-H and Ge-Cl surface bonds after HF and HCl dips, respectively. In addition, these aqueous etchants could lead to oxide-free surface, especially for high etchant concentrations [23,30,31]. However, a few reports contradicted these results, demonstrating a residual (sub)oxide contamination after both highly concentrated HF and HCl treatments [32–35]. In parallel, a few reports were focused on the ambient stability of the surface bonds [23,29,34,35]. However, these reports exhibit contradictory results concerning the ambient stability. The impact of these etchants on the Ge surface band structure is marginally studied and exhibits inconsistent results. Park *et al.*[36] reported a positive band bending after halogenated acid cleaning. Other reports mentioned negative band curvature [37] or quasi-flat band situation [38]. Aside from these surface investigations, the effectiveness of these two treatments for enhancing the minority carrier lifetime is also demonstrated [39]. Despite these reports on halide passivation, certain aspects remain ambiguous. Firstly, some authors mentioned a high Ge reactivity with

ambient air [27], but the evolution of the surface chemical properties with air exposure dependence is barely investigated and shows inconsistent outcomes, while this air exposure is quasi-inevitable in real semiconductor processing, and a proper control of this air exposure is required for surface passivation viability. Secondly, the modification of the band structure after halogenated acid treatment remains to be clarified, especially after HCl cleaning. Thirdly, the influence of an air exposure on the electronic band structure, which would impact both device performances and reliability [38], has not been reported to date. Lastly, the origin of the minority carrier lifetime's enhancement has not been clarified.

In this work, we present a comprehensive comparison between HF and HCl cleaning procedures on p-type Ge (100) surfaces and elucidate the modification of both the surface composition and the electronic band structure after these treatments by parallel Angle-resolved X-ray Photoelectron Spectroscopy (AR-XPS) measurements. In addition, their evolutions with air exposure dependence are clarified. Finally, we use Microwave Detected Photoconductivity (MDP) measurements to study the influence of these halide treatments and their relative surface modifications on the minority carrier lifetime.

II. EXPERIMENTAL

A. Samples

P-type gallium-doped, 50 mm diameter Ge wafers with a resistivity of 5-15 Ω.cm and (100) crystal orientation with a 6° miscut towards (111), as well as hydrofluoric acid (HF, 49 wt.%), hydrochloric acid (HCl, 37 wt.%), and ultra-pure water (H_2O), are used in this study. Ge samples received two treatments: either HF or HCl for 5 min. For HF-treated samples, a water rinse for 1 min has been added for safety reasons. After each

cleaning procedure, the samples were dried by a nitrogen gun. To study the influence of oxide regrowth (the queue time), the samples were left in the ambient air in a cleanroom with 45% humidity and 21°C.

B. Material characterizations

The chemical composition as well as the surface band structure are investigated with parallel Angle-resolved X-ray Photoelectron Spectroscopy (AR-XPS, Thermo Avantage Theta 300). X-ray photons are generated with a monochromatic Al Kα X-ray source (1486.6 eV). The angular mode uses eight angles regularly spaced between 23.75° and 76.25°, referred to the normal of the wafer (*i.e.*, collection angles). The angles of 23.75° and 76.25° correspond to photoelectrons escaping from the bulk and near-surface with a probed depth of about 8 nm and 2 nm, respectively. The XPS step size is 0.05 eV, the pass energy and dwell time are set at 60 eV and 500 ms, respectively [40].

To investigate the surface composition and band structure after wet cleaning, the angle of 76.25° is used to have a better surface sensitivity. The atomic composition depth profiles from AR-XPS data were reconstructed with an algorithm based on the maximum entropy method (provided by Thermo Fischer Scientific) [41]. We investigated the Ge*3d*, O*1s*, C*1s*, Cl*2p,* and F*1s* core-level spectra for this study to extract concentrations of Ge, O, C, Cl, and F, respectively. Avantage™ software was used to decompose and fit all the peaks. The background was subtracted using a Shirley function, and element concentration was obtained by dividing the peak area by the corresponding Al Scofield cross-section coefficients. All XPS spectra were referenced in energy by positioning the C*1s* peak at 284.8 eV to account for any charging shifts [42].

Another valuable parameter for further surface modification is the surface electronic structure. This structure is determined by measuring the valence band maximum energy (E_{VBM}) using the ARXPS. The XPS spectrum with the 76.25° collecting angle in the energy region of 0-15 eV corresponds to the Ge surface valence band spectrum. This range can be used to evaluate the E_{VBM} by linear extrapolation of the XPS low binding energy cut-off [43]. From these values, the band bending with respect to the Fermi level can be determined. The wafer's resistivity is determined by contactless conductivity measurements (SEMILAB LEI 88).

Carrier lifetimes were measured with Microwave-Detected-Photoconductivity (MDP) measurements setup from Freiberg Instruments, with a laser diode with a 980 nm emission line, a power of 90 mW, and a spot diameter of 1 mm. The measured lifetimes are used to estimate the surface recombination velocity (SRV) after each treatment with the following equation (Eq. 1) [17]:

$$SRV = \left(\frac{1}{\tau_{eff}} - \frac{1}{\tau_{bulk}}\right).\frac{W}{2} \sim \frac{W}{2\tau_{eff}} \qquad (\mathbf{1})$$

With SRV in cm/s, W the thickness of the wafer, τ_{eff} and τ_{bulk} the effective lifetime and bulk lifetime, respectively. The bulk minority carrier lifetime is expected to be much larger than the effective minority carrier lifetime, leading to a minority carrier lifetime mostly driven by surface recombination [44]. In that case, the SRV values presented in this work are maximal values.

III. RESULTS AND DISCUSSION

A. *Impact of wet treatment on the surface composition and band bending of Ge*

Preliminary ARXPS experiments are performed on an as-received Ge substrate with its native oxide, hereafter referred to as *Ge as-received*. Fig. 1a shows a typical XPS Ge*3d* core-level spectrum recorded at a collection angle of 76.25°. This spectrum has been decomposed into five contributions corresponding to Ge-Ge bonds from the bulk Ge and GeO_x bonds corresponding to the four Ge surface oxidation states: Ge^{1+}, Ge^{2+}, Ge^{3+}, and Ge^{4+}. The Ge*3d* peaks related to Ge-Ge and Ge^{4+} bonds are fitted with a doublet using a spin-orbit splitting of 0.6 eV and an area ratio between the $d_{5/2}$ and $d_{3/2}$ components of 0.66. Due to the energy splitting of the Ge*3d* orbital, the doublet of the GeO_x ($1 \leq x \leq 3$) peaks is not resolved, and these contributions are fitted with a single peak. The Ge$3d_{5/2}$ peak associated with the bulk Ge-Ge bonds is located at 29.8 eV, while the peaks related to the Ge^{1+}, Ge^{2+}, Ge^{3+}, and Ge^{4+} oxidation states are shifted with respect to Ge$3d_{5/2}$ to a higher binding energy by 0.8 eV, 1.8 eV, 2.6 eV, and 3.4 eV, respectively [33]. Besides Ge, oxygen and carbon are detected on the Ge surface. The O*1s* peak (Fig. 1b) is fitted with two contributions located at 531.1 eV and 532.3 eV, which can be assigned to O-Ge-Ge and a combination of O-C and O-Ge-O (second neighbor effect) chemical environments [45], respectively, present in the native oxide and carbonaceous pollution. The reconstructed surface composition, calculated from the atomic concentration profile collected at various angles, is represented in Fig. 1c. In addition to carbon contamination, the atomic concentration profile shows that the native oxide formed on the Ge surface is 1.5 nm thick (depth at which the atomic percentage of Ge Bulk is higher than 90%). The native oxide is

mainly composed of Ge^{4+} except at the interface between the Ge oxide and Ge bulk, where the Ge^{1+} oxidation state dominates.

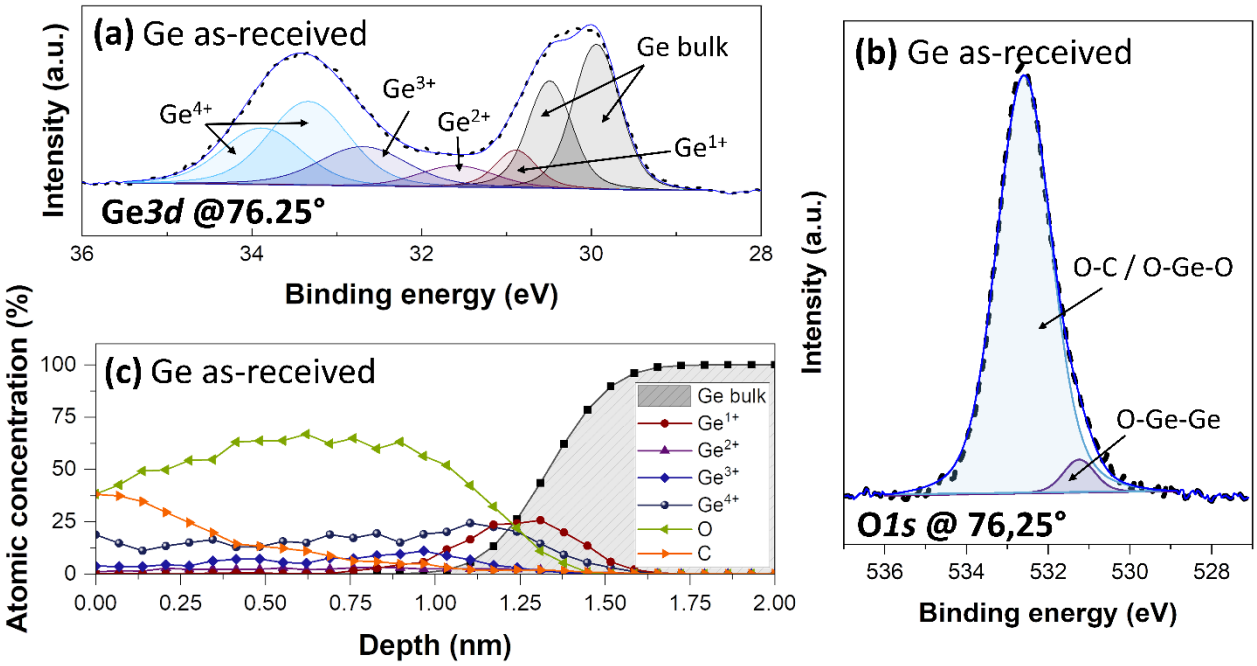

FIG. 1: XPS data for the as-received Ge sample. (a) Typical Ge*3d* peaks at a collection angle of 76.25°. (b) O*1s* spectra at a collection angle of 76.25°. (c) Atomic concentration profile as a function of the depth.

The Ge substrates are immersed either in concentrated HF for 5 minutes followed by an H_2O rinse for 1 minute, or in concentrated HCl for 5 minutes (without rinsing). XPS analyses are carried out 5 minutes after the wet dip. In both cases, the XPS analyses reveal a complete removal of Ge^{3+}- and Ge^{4+}-based compounds, as depicted in Fig. 2a and b for HF-treated and HCl-treated samples, respectively. This is also accompanied by a strong decrease in the O*1s* peak intensity (Fig. 2c). The decrease is less in the case of HF treatment, certainly because the water rinse induces a quick surface oxidation by the dissociative adsorption of H_2O [46]. After HF treatment, only traces of F-based compounds are detected (<1%, Fig. 3a). On the other side, after HCl treatment, we observe the

appearance of a Ge-Cl peak with a chemical shift of 0.6 eV, in this case [32]. The presence of this peak is confirmed by the Cl*2p* peaks located at 198.8 eV and 200.4 eV for the two spin-orbit peaks, $2p_{3/2}$ and $2p_{1/2}$, respectively (Fig. 3b). In addition, a broad peak centered at 198.5 eV, in yellow in Fig. 3b, is attributed to the Ge*3s* plasmon loss peak.

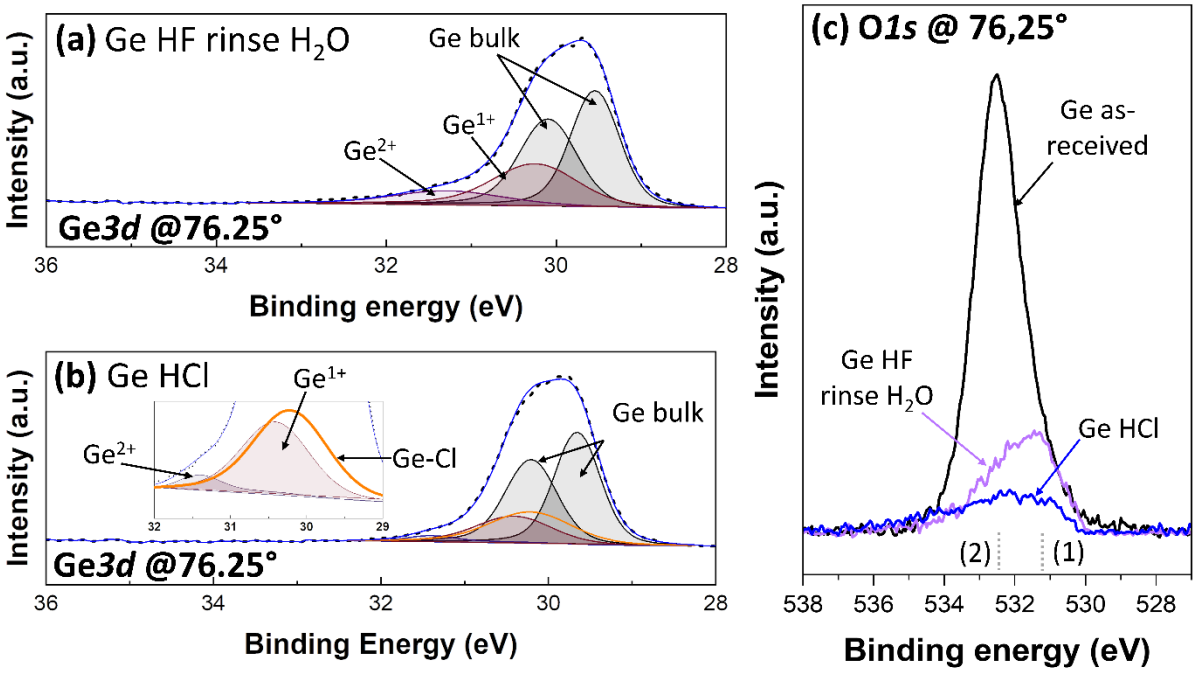

FIG. 2: XPS data after wet etching. (a) Typical Ge*3d* peaks at a collection angle of 76.25° after HF immersion for 5 min and water rinse. (b) Typical Ge*3d* peaks at a collection angle of 76.25° after HCl immersion for 5 min. (c) O*1s* spectra at a collection angle of 76.25°, the dotted lines (1) and (2) represent the peak positions of O-Ge-Ge and O-C/O-Ge-Ge, respectively.

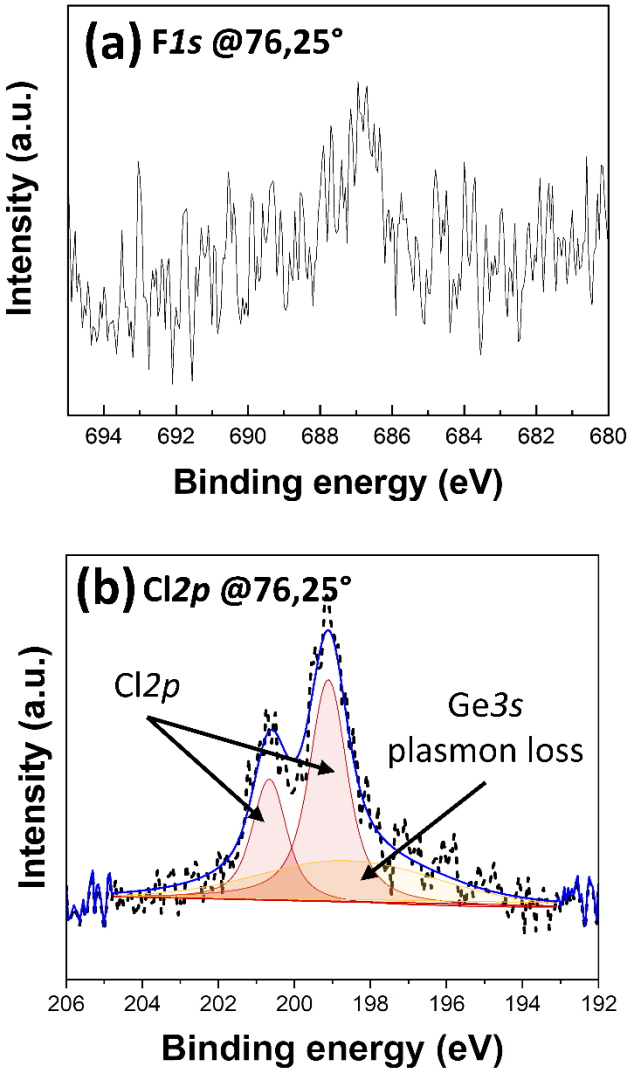

FIG. 3: (a) Typical F*1s* peaks at a collection angle of 76.25° after HF immersion for 5 min and water rinse. (b) Typical Cl*2p* peaks at a collection angle of 76.25° after HCl immersion for 5 min.

The reconstructed atomic concentration profiles after wet treatment (Fig. 4a-b) indicate that the surface layer is reduced to a 0.75 nm thickness and is mainly composed of Ge^{1+} for both treatments. In the case of HCl treatment, a Ge-Cl layer coexists with Ge^{1+}. These results confirm the capability of HF and HCl wet cleaning to remove the Ge native

oxide. The evolution of the surface composition as a function of the air exposure time has been investigated by XPS. For both HF-treated and HCl-treated samples, the Ge^{3+}- and Ge^{4+}-related peaks are visible after 110 min of queue time (air exposure), associated with a noticeable increase in the thickness of the oxide layer up to about 1 nm (Fig. 5a-b). In addition, the Ge-Cl bonds have been replaced by Ge-O bonds during the oxidation (confirmed by the disappearance of the Cl*2p* peak as showed in Fig. 5b).

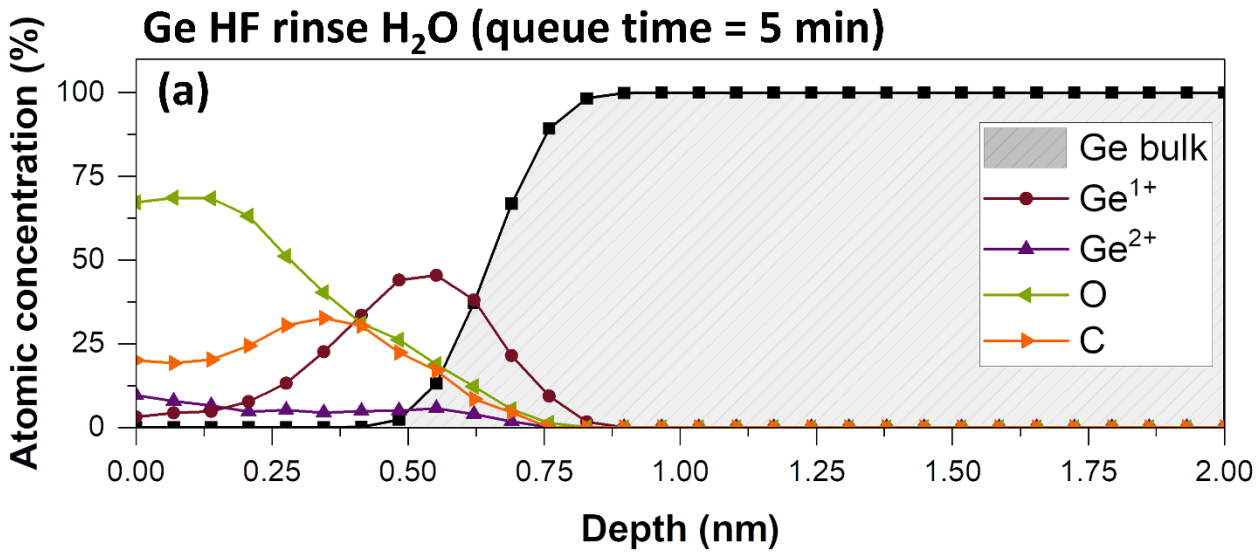

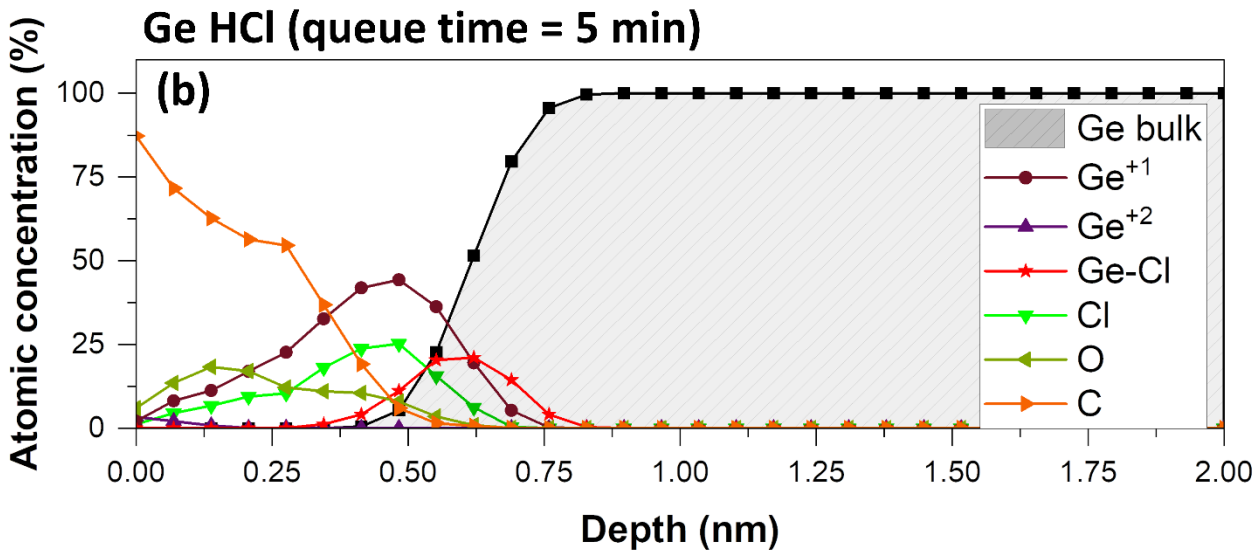

FIG. 4: Atomic concentration profiles as a function of the depth (a) after HF immersion for 5 min and water rinse, and (b) after HCl immersion for 5 min.

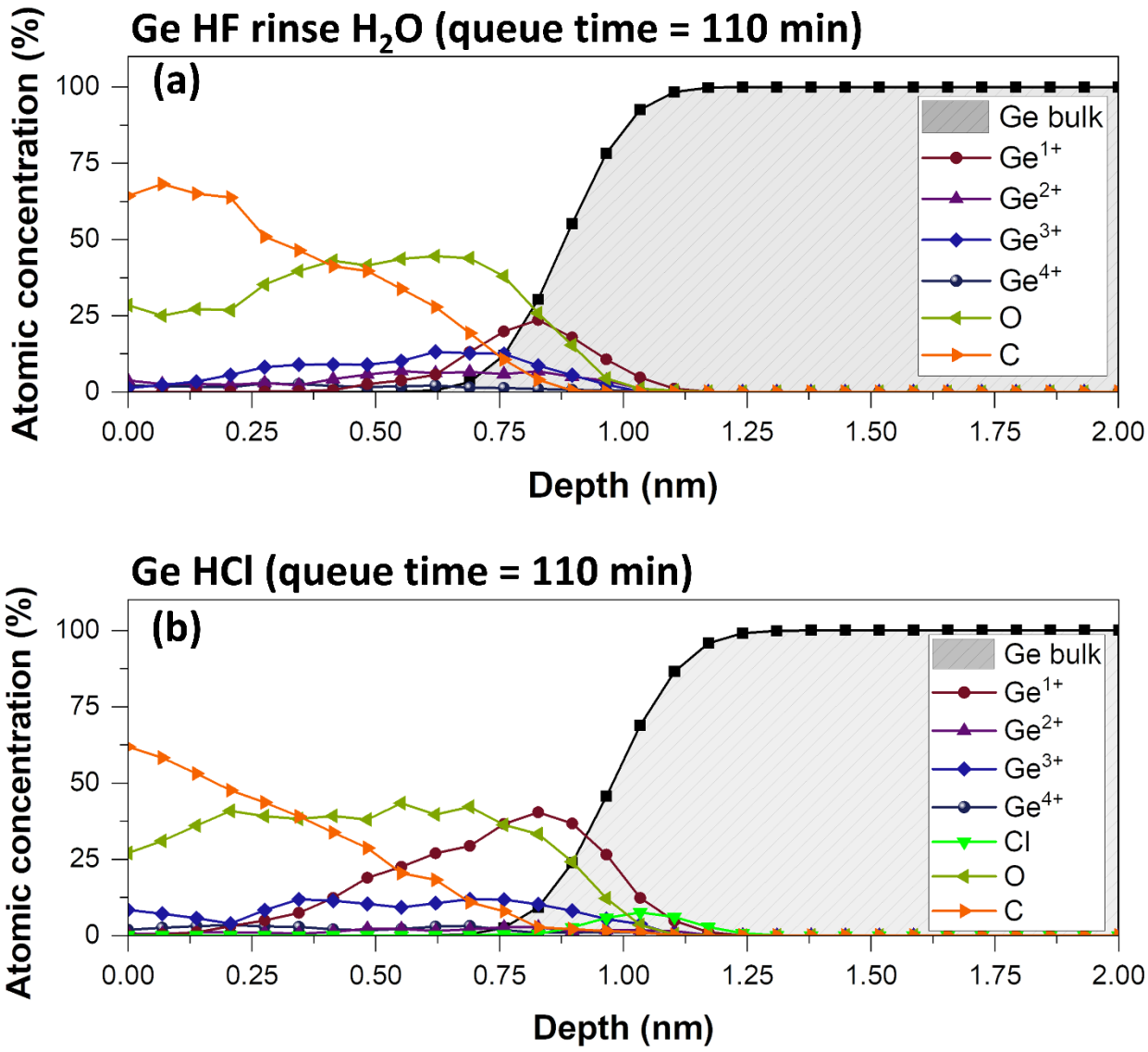

FIG. 5: Effect of air exposure. Atomic concentration profiles as a function of the depth (a) after HF treatment and 110 min of air exposure and (b) after HCl treatment and 110 min of air exposure.

To evaluate the evolution of the oxygen content in the surface layer, we calculated the average oxygen content (x) in GeO_x as a function of the air exposure time (Fig. 6), using the following equation (Eq. 2):

$$x = \frac{\sum_i i \times [I_{Ge^{i+}}]}{2 \sum_i [I_{Ge^{i+}}]} \quad (\mathbf{2})$$

Where, i is the degree of oxidation and I the peak intensity, *i.e.*, peak area, of the associated peak for the collection angle of 76.25°. Fig. 6 suggests that the oxygen content, x in GeO_x, in the surface layer is low ($x<0.7$) in a thin oxide surface layer at the beginning of the air exposure and increases as the oxide regrows. Oxygen is relatively deficient at the beginning of the air exposure, resulting in the predominance of Ge^{1+} at the Ge bulk surface in the initial state of oxidation after both treatments (Fig. 4a-b). After air exposure, the oxygen content rapidly increases, mostly due to the appearance and increase of Ge^{3+} and Ge^{4+} peaks after a few minutes of air exposure. This shows that the higher Ge oxidation states and their relative content in the surface layer increase over the course of air exposure, indicating that the surface layer is initially oxygen-deficient and becomes progressively richer in oxygen with x up to 1.05 and 1.2 for HCl- and HF-treated samples, respectively, the oxygen content will eventually approach an x value of 2 by increasing the queue time further, indicating a large majority of GeO_2 in the surface oxide layer.

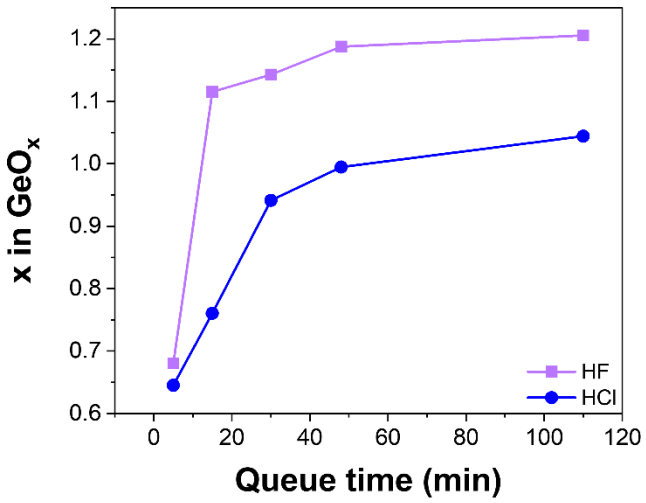

FIG. 6: O content in the oxide layer determined with Eq. 2 as a function of the queue time after HF immersion (with rinsing) and HCl immersion.

To deeply investigate the oxidation mechanism, we determined the equivalent thickness of each GeO_x compound during the air exposure in Fig. 7. The estimation of the equivalent thickness (in nm), d, for Ge-based components of the Ge*3d* core-level spectra (GeO_x and Ge-Cl) is performed by Eq.3 [47–49]:

$$d = \lambda \ln\left(1 + \frac{R_{exp}}{R_0}\right) \quad (3)$$

Where $R_{exp} = I_{GeOx}/I_{Gemet}$ with I_{GeOx} and I_{Gemet} being the measured peak intensity of the Ge*3d* peak in the oxide and metallic phases, respectively. $R_0 = {I^{\infty}_{GeOx}}/{I^{\infty}_{Gemet}}$ with I^{∞}_{GeOx} and I^{∞}_{Gemet} being the equivalent intensities for the pure bulk materials. The literature around Ge is quite limited regarding the exact value of R_0. Otherwise, the recommended value for R_0 in the case of Si and an overlayer of SiO_x is 0.93 [50]. To simplify the Eq. 3, we have fixed R_0 to be unity. λ is the corresponding photoelectron escape depth (in nm). In our case, the photoelectron emitted under the X-ray stimulation is not collected normally to the surface

but with a collecting angle set to 76.25°. The photoelectron escape depth is thus defined by Eq. 4:

$$\lambda = \Lambda\cos(\theta) \qquad (\mathbf{4})$$

Where θ is the collecting angle, and Λ is the attenuation length of the Ge*3d* electrons from the bulk and within the oxide. As the energy of the peak from Ge bulk is close to that of the GeO_x overlayer, the attenuation lengths of the Ge*3d* electron from the bulk and from the oxide are considered virtually identical. Smith *et al.* [48] have estimated Λ with the CS2 formula [51], determining a value of 2.36 nm for a GeO_2 matrix and a kinetic energy of 1456 eV. In our study, we took this value for the attenuation length. The Eq. 3 can be simplified as follows (Eq. 5) :

$$d = \Lambda\cos(\theta) \times \ln\left(1 + \frac{I_{GeOx}}{I_{Bulk}}\right) \qquad (\mathbf{5})$$

Where I_{GeOx} is the signal intensity of the oxide-related component of the Ge*3d* core-level spectrum, I_{Bulk} is the signal intensity of the corresponding bulk component.

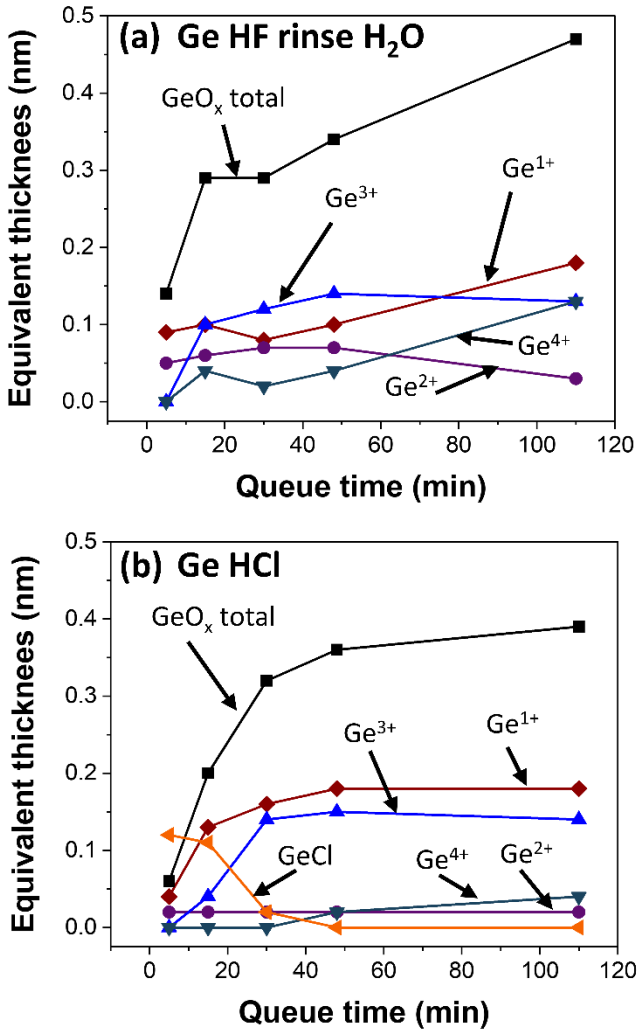

FIG. 7: Ge-based compounds' equivalent thickness extracted from XPS data: (a) after HF immersion for 5 min and water rinse, (b) after HCl immersion for 5 min.

For the HF-treated samples (Fig. 7a), the equivalent thickness of the Ge^{1+}-based compounds remains stable initially and then increases slightly after 30 min of queue time. The oxide regrowth is mainly due to the growth of Ge^{3+}-based compounds in the first steps of the oxidation and then Ge^{4+}-based compounds after 30 min of air exposure. On the other hand, for HCl-treated samples (Fig. 7b), the GeCl equivalent thickness rapidly decreases to disappear after 45 min of queue time, while at the same time the Ge^{1+} and Ge^{3+}

thicknesses increase and then stabilize. This suggests that after 45 min of queue time all the GeCl bonds are turned into GeO_x bonds, which is also consistent with the disappearance of the XPS Cl*2p* peak with the queue time as shown in Fig. 8. In comparison with the HF-treated samples, the equivalent thickness of Ge^{4+}-based compounds remains low even after 110 min of air exposure following HCl immersion. Moreover, with the HCl treatment, the Ge^{1+}-based compounds remain the dominant contribution to the oxidation over the entire period of queue time investigated here, while with HF, the amount of Ge^{1+} and Ge^{3+} in the oxidation layer is almost similar. Finally, after both treatments, the equivalent thickness of Ge^{2+}-based compounds remains low and stable throughout the oxidation process. In comparison with the *Ge as-received* sample, the equivalent thickness of Ge^{4+}-based compounds after HCl immersion is quite low even after 110 min of air exposure (d_{Ge4+} = 0.36 nm, for the as-received sample), while the equivalent thickness of the Ge^{3+}-based compounds reaches a plateau after around 30 min (d_{Ge3+} = 0.15 nm, for the as-received sample). In conclusion, at these beginning steps of the queue time, we observe a faster growth of the 3+-oxidation state, in opposition to the predominance of the 4+-oxidation state in the case of the as-received sample. After HCl immersion, the regrowth of Ge^{3+}-based compounds is slightly delayed, while virtually no regrowth is observed in Ge^{4+}-based compounds.

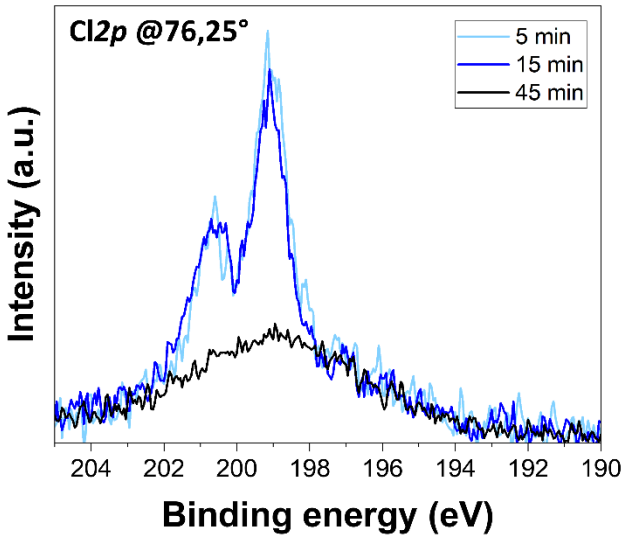

FIG. 8: Typical Cl*2p* peaks at the angle of 76.25° after HCl immersion for 5 min for three different queue times: 5 min, 15 min, and 45 min.

The band bending induced by the wet cleanings is also investigated. First, the band bending induced by the native oxide layer is determined. The intersection between the linear extrapolation of the valence band leading edge and the baseline in the binding energy region of 0-15 eV corresponding to the Ge surface valence band spectrum, indicates a valence band maximum of 0.36 eV for the *as-received* wafer (Fig. 9). For the given bulk Fermi level (E_F = 0.256 eV above E_{VBM} with the concentration of acceptor atoms, N_a = 2.87 x 10^{14} cm^{-3}, determined by wafer's resistivity measurements, ρ=12.21 Ω.cm), a slight downward band bending with a value of -0.10 ± 0.05 eV is observed for the *as-received* sample (Fig. 10a). After determining this "native" band bending value, the band bending after both treatments is measured and compared to the band bending of the as-received Ge sample. After oxide removal, for either HF- or HCl-treated samples, the E_{VBM} exhibits lower values than the reference with 0.06 eV and 0.19 eV after HF and HCl immersion, respectively. This indicates a positive band bending after both treatments. The HF-treated

sample exhibits a higher positive band bending with a value of +0.20 ± 0.05 eV (Fig. 10b), indicating a higher level of field-effect passivation after HF immersion. Conversely, the HCl-treated sample exhibits a lower positive band bending with a value of +0.07 ± 0.05 eV (Fig. 10c).

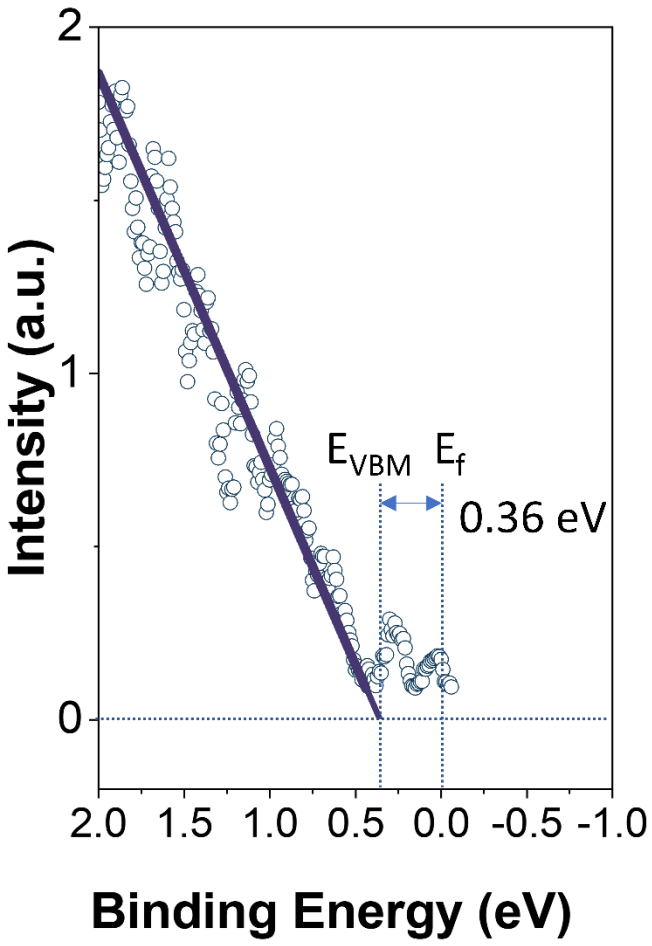

FIG. 9: Representative E_{VBM} measurement for band bending determination of Ge reference sample (*as received*).

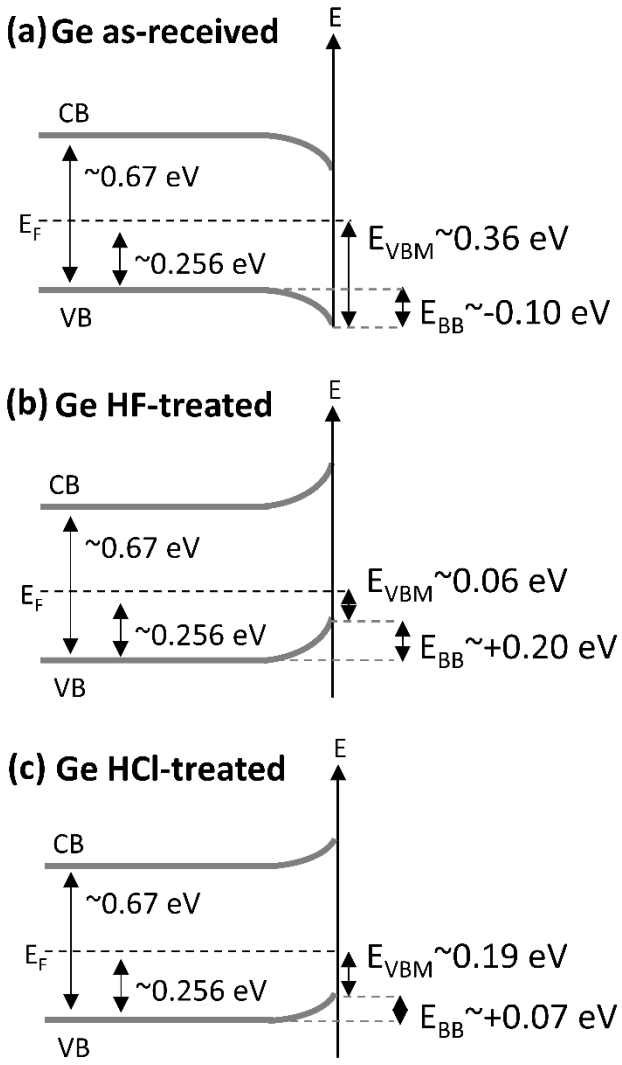

FIG. 10: Schematic illustrations of the band bending for (a) the as-received sample, (b) after HF immersion and water rinsing and (c) after HCl immersion, respectively. The band bending values are determined after 5 min of air exposure.

The band bending at the surface is a combined effect caused by multiple charged defects and should satisfy the charge neutrality. Two different types of charges should be considered [52]: (1) $Q_{s,}$ are the semiconductor surface charges resulting from the band bending, (2) Q_{surf}, are the fixed surface charges. The latter, in the absence of an external electric field, can be separated into three different contributions: the net charged interface traps, which are negatively charged [53], the net positive charges accumulated in the oxide

layer [54], and the net charges induced by the surface bond's dipole moment. Due to the interface's net surface charges (Q_{surf}), the band will bend close to the interface and induce an accumulation (positive band bending) or depletion (negative band bending) of holes. As a result, we assumed that the different band bending between HF- and HCl-treated samples just after immersion is twofold. First, after immersion, we have determined that the surface layer is oxygen-deficient (Fig. 6). This oxygen-deficient layer is known to induce negative interface states formed by a dangling bond at a Ge atom back-bonded to two other Ge atoms and one oxygen atom ($Ge_2O{\equiv}Ge\cdot$)[55]. After HCl treatment, the presence of Ge-Cl bonds close to the interface with the bulk material could chemically passivate the interface states induced by the Ge^{+1}-based compounds and reduce their number, as depicted in Fig. 7b. In addition, the different surface bonds between HF- and HCl-treated samples can induce a different dipole moment. It is possible to estimate the dipole moment (μ_0) of a surface bond with the following equation [56] (Eq. 6):

$$\mu_0 = e_0 \sum r_{cov} \left(0.16|X_A - X_B| + 0.035(X_A - X_B)^2\right) \qquad (\mathbf{6})$$

With e_0, the electric charge, r_{cov}, and X represent the covalent radius and electronegativity of the two elements involved in the bond, respectively. A dipole moment of 2.9 D for the Ge-O bond and 2.6 D for the Ge-Cl bond is determined. This difference induces a lower negative charge at the surface in the case of the HCl-treated sample. In addition, Fig. 3 shows traces of F on the surface of our sample. We attribute these F-based compounds to Ge-F bonds. The formation of Ge-F is barely possible due to thermodynamic considerations; however, there is a non-zero probability, as recently demonstrated on Si 55. In this case, this very small proportion of Ge-F could induce a high positive band bending due to a dipole moment of 5.6 D. Finally, due to the lower concentration of Ge^{1+}-

based compounds, the reduced dipole moment of the Ge-Cl bonds compared to Ge-O and Ge-F bonds, and the potential chemical passivation induced by these bonds, the Q_{surf} is lower after HCl immersion, which results a lower Q_s due to the charge conservation and, therefore, a reduced surface band bending.

The Fig. 11a depicts the band bending evolution as a function of the air exposure duration after both deoxidations. With air exposure, the band bending decreases after the HF treatment to reach a value close to the one obtained for the as-received sample. We attribute this decrease to the increase in the density of positive fixed charges in the oxide layer due to the Ge^{4+} regrowth. These positive fixed charges will counteract the surface charges induced by the bonds at the interface with the bulk material and by surface states. In parallel, band bending is represented as a function of the total equivalent thickness of GeO_x-based compounds, determined with Eq. 5, in Fig. 11b. Interestingly, a threshold between 0.3 nm and 0.4 nm in total oxide compound thickness seems to result in a significant decrease in band bending. Therefore, we propose that at low GeO_x equivalent thicknesses (<0.4 nm), band bending is controlled by the dipole-induced charges of functional groups at the surface of Ge and interface states, while at higher thickness, fixed positive charges in the regrown Ge^{4+}-based compound control band bending and lead to a lower band bending, proportional to the GeO_x equivalent thickness.

On the other hand, the HCl-treated sample exhibits a slight increase in the band bending until 45 minutes of air exposure, followed by a decrease for longer times (Fig. 11a). This increase could be induced by the oxidation of Ge-Cl bonds into Ge-O bonds. Interestingly, the band bending remains quite stable and positive after the HCl immersion even after 110 min of air exposure. This delay could be related to the delayed Ge^{4+}-based

compounds' regrowth after HCl immersion in comparison with the HF (Fig. 7). Lastly, the band bending as a function of the total GeO_x-based compounds' equivalent thickness seems to follow the same trend as the one observed for the HF-treated sample, exhibiting a threshold of around 0.3 to 0.4nm, however, as the HCl-treated sample exhibits a very low regrowth of Ge^{4+}-based compounds, the band bending remains quite stable in the time domain investigated here, with a slight decrease observed after 0.35 nm of the total equivalent thickness of GeOx-based compounds.

To conclude our XPS investigations, both HF and HCl treatments have strengths and weaknesses. Depending on the user's requirements, surface composition can be favored by using HCl, which provides better oxide and suboxide elimination with chemical passivation by Ge-Cl bonds. Additionally, the growth of Ge4+ is delayed in comparison with HF, resulting in a positive and stable band bending even after 110 minutes of air exposure. Conversely, HF treatment could be favored for the higher positive band bending it provides.

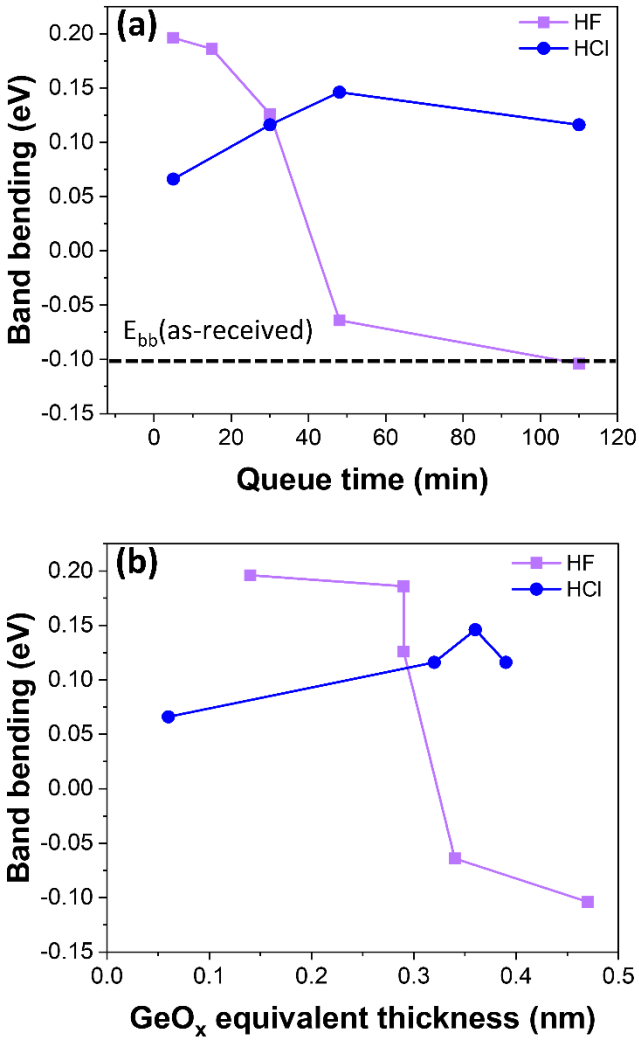

FIG. 11: (a) Band bending as a function of the queue time. (b) The band bending value as a function of the total GeOx-based equivalent thickness for the HF-treated sample.

B. Impact on the minority carrier lifetime and recombination velocity

To investigate the impact of both chemical and electronic structure on the Ge surface passivation, the minority carrier lifetime is determined after both HF treatment (with rinsing) and HCl treatment (without rinsing) in Fig. 12. The lifetime is monitored until 100 min of queue time. For the bare Ge surface with a native oxide (as-received

sample, horizontal dotted line in Fig. 12), a low minority carrier lifetime of 50 µs, corresponding to a high surface recombination velocity (SRV, Eq. 1) of 175 cm/s is observed. For HF deoxidation (with rinsing), a minority carrier lifetime of ~ 200 µs (SRV ~ 35 cm/s) is measured immediately after treatment. This value rapidly decreases with air exposure duration, down to 60 µs after 100 minutes of air exposure, which is close to the minority carrier lifetime of the as-received sample. After HCl-based deoxidation and 5 min air exposure, the minority carrier lifetime is 350 µs (SRV ~ 35 cm/s), which is in accordance with previous reports [39]. Surprisingly, the lifetime value is higher than with HF deoxidation, even though the band bending is less favorable. The higher coverage of Ge^{+1} depicted after HF immersion (Fig. 7a) is known to increase the defect density, reducing the chemical passivation which seems to dominate the surface passivation mechanism here. Interestingly, the decrease in lifetime seems to be delayed after HCl immersion. According to Fig. 7b, this delay is likely due to the strong increase in Ge^{1+}-based compounds equivalent thickness during the oxide regrowth process mostly due to the oxidation process of Ge-Cl bonds. In addition, as depicted in Fig. 11a, the band bending remains quite stable. It allows for reaching a maximum carrier lifetime value (~ 380 µs) after around 10 min of air exposure. This could be interesting for device processing by relaxing the queue time constraint in the manufacturing line. Finally, with longer air exposure, the carrier lifetime decreases to 70 µs after 100 min, slightly above the one of the references samples.

To combine both favorable chemical passivation and high positive band bending, we investigated HF immersion for 5 min without rinsing. After this treatment, the minority carrier lifetime exceeds 800 µs (SRV ~ 11 cm/s). This value is higher than the one obtained after diluted HF (2-3%) treatment [39]. This remarkably value is attributed to the low defect

density at the Ge/GeO_x interface after HF cleaning, possibly due to the presence of Ge-H bonds [58–60]. Moreover, we expect a lower density of GeO_x than in the case of the water rinse. Finally, we suppose a high positive band bending due to the presence of Ge-F bonds. We expect a higher probability of Ge-F bond formation without the water rinse. In this case, this proportion of Ge-F could induce a high positive band bending due to a dipole moment of 5.6 D. Unfortunately, due to safety limitations at the XPS testing site, these assumptions could not be verified in our XPS setup and remain to be confirmed.

Our lifetime investigations provide insights into the impact of both chemical and field-effect passivation, provided by both surface composition and band bending modifications induced by HF and HCl treatments. The water rinse seems to be highly detrimental to surface passivation in the case of HF, mostly due to the dissociative adsorption of H_2O, probably inducing a modification of both surface composition and electronic structure. For passivation purposes, our investigation would recommend using concentrated HF without water rinsing to maximize the field-effect passivation, which greatly impacts surface passivation.

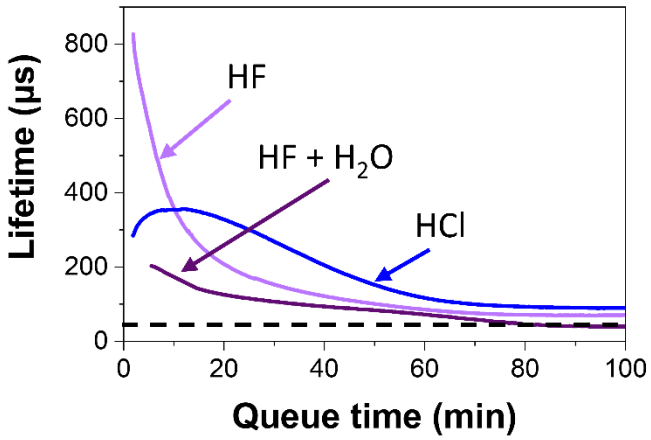

FIG. 12: Lifetime as a function of the air exposure for HF (without rinsing), HCl (without rinsing), and HF+H_2O treatment. The dotted line represents the lifetime our the *as-received* sample.

IV. CONCLUSIONS

The results presented in this study demonstrate that the cleaning procedure plays a critical role in the chemical composition, the surface band structure, the oxidation resistance, and the minority carrier lifetime of Ge. Our findings revealed varying oxide regrowth behaviors. For instance, Ge samples treated with HF exhibited a rapid regrowth of all degrees of oxidation, while those treated with HCl showed a reduced concentration of low degrees of oxidation following the cleaning and slower or negligible regrowth of high degrees of oxidation, even after 110 minutes of air exposure. This difference can be attributed to the presence of Ge-Cl bonds, which induce a distinct oxidation process compared to the Ge-OH bonds resulting from HF cleaning. As a consequence of these distinct surface compositions, Ge subjected to HF treatment with a water rinse displayed a pronounced positive band bending of +0.20 eV. In contrast, HCl-treated samples exhibited a lower band curvature of +0.07 eV, primarily due to the presence of Ge-Cl bonds on the Ge surface. Over the course of air exposure, an increase in the coverage of GeOx-based compounds led to a significant reduction in band bending after HF treatment, while HCl treatment maintained a consistent band bending. In summary, these factors collectively contributed to a reduction in the surface recombination velocity (SRV) after wet etching. By combining chemical and field-induced passivation, we achieved a minority carrier lifetime exceeding 800 μs in HF-treated germanium without rinsing.

Our findings underscore the role of an effective chemical surface cleaning procedure in ensuring the optimal Ge surface passivation, shedding light on the temporal evolution under air exposure of the chemical composition, surface band structure, oxidation

resistance, and minority carrier lifetime. These findings emphasize the critical impact of the cleaning procedure on the performance of Ge surfaces, thereby highlighting the significance of careful surface treatment for enhanced device efficiency.

ACKNOWLEDGMENTS

The authors thank and the 3IT's clean room staff for technical support. The authors also thank the Natural Sciences and Engineering Research Council of Canada (NSERC), Innovation en énergie électrique (InnovÉÉ), Mitacs, Umicore and Saint-Augustin Canada Electric (Stace) for financial support. LN2 is a joint International Research Laboratory (IRL 3463) funded and co-operated in Canada by Université de Sherbrooke and in France by CNRS as well as ECL, INSA Lyon, and Université Grenoble Alpes (UGA). It is also supported by the Fonds de Recherche du Québec Nature et Technologie (FRQNT). This work was supported by the French Government program "Investissements d'Avenir" managed by the National Research Agency (ANR) under the Contract No. ANR-10-EQPX-33. The authors also thank the French RENATECH network.

AUTHOR DECLARATIONS

Conflict of interest

The authors have no conflicts to disclose.

DATA AVAILABILITY

The data that support the findings of this study are available from the corresponding author upon reasonable request.

CREDIT AUTHOR STATEMENT

The manuscript was written through contributions of all authors. All authors have given approval to the final version of the manuscript. **A.Chapotot.:** Conceptualization (equal), Methodology (equal), Formal analysis (lead), Investigation (equal), Original Draft (lead), Review & Editing (equal), Visualization (lead). **J.Chrétien:** Conceptualization (supporting), Methodology (equal), Investigation (equal), Review & Editing (supporting), Supervision (equal). **O.Fesiienko:** Methodology (equal), Review & Editing (supporting), Investigation (equal). **E.Pargon:** Conceptualization (supporting), Methodology (equal), Review & Editing (equal), Supervision (equal). **J.Cho, K.Dessein.:** Review & Editing (supporting). **A.Boucherif, G.Hamon, :** Supervision (equal), Review & Editing (supporting), Funding acquisition (equal) **M.Darnon:** Conceptualization (equal), Supervision (equal), Review & Editing (equal), Funding acquisition (equal).

REFERENCES

[1] R. Pillarisetty, "Academic and industry research progress in germanium nanodevices," Nature **479**(7373), 324–328 (2011).
[2] M.R.M. Atalla, S. Assali, A. Attiaoui, C. Lemieux-Leduc, A. Kumar, S. Abdi, and O. Moutanabbir, "All-Group IV Transferable Membrane Mid-Infrared Photodetectors," Adv. Funct. Mater. **31**(3), 2006329 (2021).
[3] N. Paupy, Z. Oulad Elhmaidi, A. Chapotot, T. Hanuš, J. Arias-Zapata, B. Ilahi, A. Heintz, A.B. Poungoué Mbeunmi, R. Arvinte, M.R. Aziziyan, V. Daniel, G. Hamon, J. Chrétien, F. Zouaghi, A. Ayari, L. Mouchel, J. Henriques, L. Demoulin, T.M. Diallo, P.-O. Provost, H. Pelletier, M. Volatier, R. Kurstjens, J. Cho, G. Courtois, K. Dessein, S. Arcand, C. Dubuc, A. Jaouad, N. Quaegebeur, R. Gosselin, D. Machon, R. Arès, M. Darnon, and A. Boucherif, "Wafer-scale detachable monocrystalline germanium nanomembranes for the growth of III–V materials and substrate reuse," Nanoscale Adv., 10.1039.D3NA00053B (2023).
[4] T. Hanuš, B. Ilahi, A. Chapotot, H. Pelletier, J. Cho, K. Dessein, and A. Boucherif, "Wafer-scale Ge freestanding membranes for lightweight and flexible optoelectronics," Mater. Today Adv. **18**, 100373 (2023).
[5] Z. Xia, H. Song, M. Kim, M. Zhou, T.-H. Chang, D. Liu, X. Yin, K. Xiong, H. Mi, X. Wang, F. Xia, Z. Yu, Z. (Jack) Ma, and Q. Gan, "Single-crystalline germanium nanomembrane photodetectors on foreign nanocavities," Sci. Adv. **3**(7), e1602783 (2017).
[6] D. Ren, C. Dong, S.J. Addamane, and D. Burghoff, "High-quality microresonators in the longwave infrared based on native germanium," Nat. Commun. **13**(1), 5727 (2022).
[7] S.P. Adiga, C. Jin, L.A. Curtiss, N.A. Monteiro-Riviere, and R.J. Narayan, "Nanoporous membranes for medical and biological applications: Nanoporous membranes for medical and biological applications," Wiley Interdiscip. Rev. Nanomed. Nanobiotechnol. **1**(5), 568–581 (2009).
[8] A. Dupuy, A. Roland, M.R. Aziziyan, S. Sauze, D. Machon, R. Arès, and A. Boucherif, "Monolithic integration of mesoporous germanium: A step toward high-performance on-chip anode," Mater. Today Commun. **26**, 101820 (2021).
[9] R.R. King, D.C. Law, K.M. Edmondson, C.M. Fetzer, G.S. Kinsey, H. Yoon, R.A. Sherif, and N.H. Karam, "40% efficient metamorphic GaInP⁄GaInAs⁄Ge multijunction solar cells," Appl. Phys. Lett. **90**(18), 183516 (2007).
[10] Q. Xie, S. Deng, M. Schaekers, D. Lin, M. Caymax, A. Delabie, X.-P. Qu, Y.-L. Jiang, D. Deduytsche, and C. Detavernier, "Germanium surface passivation and atomic layer deposition of high- *k* dielectrics—a tutorial review on Ge-based MOS capacitors," Semicond. Sci. Technol. **27**(7), 074012 (2012).
[11] J. Sun, and J. Lu, "Interface Engineering and Gate Dielectric Engineering for High Performance Ge MOSFETs," Adv. Condens. Matter Phys. **2015**, 1–9 (2015).
[12] G. Dingemans, P. Engelhart, R. Seguin, F. Einsele, B. Hoex, M.C.M. van de Sanden, and W.M.M. Kessels, "Stability of Al2O3 and Al2O3/a-SiNx:H stacks for surface passivation of crystalline silicon," J. Appl. Phys. **106**(11), 114907 (2009).
[13] Y.-Y. Chen, H.-C. Chang, Y.-H. Chi, C.-H. Huang, and C.W. Liu, "$\hbox{GeO}_{2}$ Passivation for Low Surface Recombination Velocity on Ge Surface," IEEE Electron Device Lett. **34**(3), 444–446 (2013).

[14] W.J.H. Berghuis, J. Melskens, B. Macco, R.J. Theeuwes, M.A. Verheijen, and W.M.M. Kessels, "Surface passivation of germanium by atomic layer deposited Al2O3 nanolayers," J. Mater. Res. **36**(3), 571–581 (2021).
[15] W.J.H. (Willem-J. Berghuis, J. Melskens, B. Macco, R.J. Theeuwes, L.E. Black, M.A. Verheijen, and W.M.M. (Erwin) Kessels, "Excellent surface passivation of germanium by a-Si:H/Al_2O_3 stacks," J. Appl. Phys. **130**(13), 135303 (2021).
[16] W.J.H. (Willem-J. Berghuis, M. Helmes, J. Melskens, R.J. Theeuwes, W.M.M. (Erwin) Kessels, and B. Macco, "Extracting surface recombination parameters of germanium–dielectric interfaces by corona-lifetime experiments," J. Appl. Phys. **131**(19), 195301 (2022).
[17] J. Isometsä, T.H. Fung, T.P. Pasanen, H. Liu, M. Yli-koski, V. Vähänissi, and H. Savin, "Achieving surface recombination velocity below 10 cm/s in *n* -type germanium using ALD Al_2O_3," APL Mater. **9**(11), 111113 (2021).
[18] J. Isometsä, Z. Jahanshah Rad, T.H. Fung, H. Liu, J.-P. Lehtiö, T.P. Pasanen, O. Leiviskä, M. Miettinen, P. Laukkanen, K. Kokko, H. Savin, and V. Vähänissi, "Surface Passivation of Germanium with ALD Al2O3: Impact of Composition and Crystallinity of GeOx Interlayer," Crystals **13**(4), 667 (2023).
[19] N.E. Posthuma, G. Flamand, W. Geens, and J. Poortmans, "Surface passivation for germanium photovoltaic cells," Sol. Energy Mater. Sol. Cells **88**(1), 37–45 (2005).
[20] C. Weiss, J. Schön, O. Höhn, B. Fuhrmann, F. Dimroth, and S. Janz, "Passivated, Highly Reflecting, Laser Contacted Ge Rear Side for III-V Multi-Junction Solar Cells," IEEE J. Photovolt. **11**(5), 1256–1263 (2021).
[21] S. Janz, C. Weiss, C. Mohr, R. Kurstjens, B. Boizot, B. Fuhrmann, and V. Khorenko, in *2017 IEEE 44th Photovolt. Spec. Conf. PVSC* (IEEE, Washington, DC, USA, 2017), pp. 83–87.
[22] A. Chapotot, B. Ilahi, J. Arias-Zapata, T. Hanuš, A. Ayari, G. Hamon, J. Cho, K. Dessein, M. Darnon, and A. Boucherif, "Germanium surface wet-etch-reconditioning for porous lift-off and substrate reuse," Mater. Sci. Semicond. Process. **168**, 107851 (2023).
[23] S. Rivillon, Y.J. Chabal, F. Amy, and A. Kahn, "Hydrogen passivation of germanium (100) surface using wet chemical preparation," Appl. Phys. Lett. **87**(25), 253101 (2005).
[24] H. Okumura, T. Akane, and S. Matsumoto, "Carbon contamination free Ge(100) surface cleaning for MBE," Appl. Surf. Sci. **125**(1), 125–128 (1998).
[25] G. Collins, D. Aureau, J.D. Holmes, A. Etcheberry, and C. O'Dwyer, "Germanium Oxide Removal by Citric Acid and Thiol Passivation from Citric Acid-Terminated Ge(100)," Langmuir **30**(47), 14123–14127 (2014).
[26] D. Bodlaki, H. Yamamoto, D.H. Waldeck, and E. Borguet, "Ambient stability of chemically passivated germanium interfaces," Surf. Sci. **543**(1–3), 63–74 (2003).
[27] P. Ponath, A.B. Posadas, and A.A. Demkov, "Ge(001) surface cleaning methods for device integration," Appl. Phys. Rev. **4**(2), 021308 (2017).
[28] K. Choi, and J.M. Buriak, "Hydrogermylation of Alkenes and Alkynes on Hydride-Terminated Ge(100) Surfaces," Langmuir **16**(20), 7737–7741 (2000).
[29] S. Sun, Y. Sun, and Z. Liu, "Surface termination and roughness of Ge(100) cleaned by HF and HCl solutions," Appl Phys Lett, 4 (n.d.).
[30] S.R. Amy, Y.J. Chabal, F. Amy, A. Kahn, C. Krugg, and P. Kirsch, "Wet Chemical Cleaning of Germanium Surfaces for Growth of High-k Dielectrics," MRS Proc. **917**, 0917-E01-05 (2006).

[31] T. Deegan, and G. Hughes, “An X-ray photoelectron spectroscopy study of the HF etching of native oxides on Ge(111) and Ge(100) surfaces,” Appl. Surf. Sci. **123–124**, 66–70 (1998).
[32] G.H.A. Abrenica, M. Fingerle, M.V. Lebedev, S. Arnauts, T. Mayer, F. Holsteyns, S. de Gendt, and D.H. van Dorp, “Wet Chemical Processing of Ge in Acidic H_2O_2 Solution: Nanoscale Etching and Surface Chemistry,” ECS J. Solid State Sci. Technol. **9**(8), 084002 (2020).
[33] T.M. Diallo, M.R. Aziziyan, R. Arvinte, R. Arès, S. Fafard, and A. Boucherif, “CVD growth of high-quality graphene over Ge (100) by annihilation of thermal pits,” Carbon **174**, 214–226 (2021).
[34] B. Onsia, M. Caymax, T. Conard, S. De Gendt, F. De Smedt, A. Delabie, C. Gottschalk, M.M. Heyns, M. Green, S. Lin, P.W. Mertens, W. Tsai, and C. Vinckier, “On the Application of a Thin Ozone Based Wet Chemical Oxide as an Interface for ALD High-k Deposition,” Solid State Phenom. **103–104**, 19–22 (2005).
[35] J.Y. Kim, J. McVittie, K. Saraswat, and Y. Nishi, “Passivation Studies of Germanium Surfaces,” Solid State Phenom. **134**, 33–36 (2007).
[36] S.J. Park, L. Bolotov, N. Uchida, and T. Tada, “Distribution of free carriers near heavily-doped epitaxial surfaces of n-type Ge(100) upon HF and HCl treatments,” AIP Adv. **5**(10), 107219 (2015).
[37] C. Fleischmann, K. Schouteden, M. Müller, P. Hönicke, B. Beckhoff, S. Sioncke, H.-G. Boyen, M. Meuris, C. Van Haesendonck, K. Temst, and A. Vantomme, “Impact of ammonium sulfide solution on electronic properties and ambient stability of germanium surfaces: towards Ge-based microelectronic devices,” J. Mater. Chem. C **1**(26), 4105 (2013).
[38] W. Zhang, X. Lou, Z. Xie, and H. Chang, “Band bending analysis of charge characteristics at GeO_2/Ge interface by x-ray photoemission spectroscopy,” J. Phys. Appl. Phys. **52**(4), 045101 (2019).
[39] B.P. Swain, H. Takato, Z. Liu, and I. Sakata, “Ambient stability of wet chemically passivated germanium wafer for crystalline solar cells,” Sol. Energy Mater. Sol. Cells **95**(1), 84–88 (2011).
[40] L. Edwards, P. Mack, and D.J. Morgan, “Recent advances in dual mode charge compensation for XPS analysis,” Surf. Interface Anal. **51**(9), 925–933 (2019).
[41] C.R. Brundle, in *AIP Conf. Proc.* (AIP, Richardson, Texas (USA), 2005), pp. 307–313.
[42] R. Sohal, P. Dudek, and O. Hilt, “Comparative study of NH4OH and HCl etching behaviours on AlGaN surfaces,” Appl. Surf. Sci. **256**(7), 2210–2214 (2010).
[43] O. Fesiienko, C. Petit-Etienne, M. Darnon, A. Soltani, H. Maher, and E. Pargon, “Plasma induced damage on AlGaN/GaN heterostructure during gate opening for power devices,” J. Vac. Sci. Technol. A **41**(3), 033004 (2023).
[44] K.R. McIntosh, and L.E. Black, “On effective surface recombination parameters,” J. Appl. Phys. **116**(1), 014503 (2014).
[45] K. Prabhakaran, and T. Ogino, “Oxidation of Ge(100) and Ge(ll 1) surfaces: an UPS and XPS study,” 9 (n.d.).
[46] H.J. Kuhr, and W. Ranke, “H2O adsorption on a cylindrical germanium sample,” Surf. Sci. **187**(1), 98–111 (1987).

[47] A. Jablonski, and J. Zemek, "Overlayer thickness determination by XPS using the multiline approach: Overlayer thickness determination by XPS using the multiline approach," Surf. Interface Anal. **41**(3), 193–204 (2009).
[48] E.F. Smith, D. Briggs, and N. Fairley, "Further developments in quantitative X-ray photoelectron spectromicroscopy: preliminary results from the study of germanium corrosion," Surf. Interface Anal. **38**(2), 69–75 (2006).
[49] M.P. Seah, and S.J. Spencer, "Ultrathin SiO2 on Si II. Issues in quantification of the oxide thickness," Surf. Interface Anal. **33**(8), 640–652 (2002).
[50] M.P. Seah, and S.J. Spencer, "Ultrathin SiO2 on Si IV. Intensity measurement in XPS and deduced thickness linearity," Surf. Interface Anal. **35**(6), 515–524 (2003).
[51] P.J. Cumpson, and M.P. Seah, "Elastic Scattering Corrections in AES and XPS. II. Estimating Attenuation Lengths and Conditions Required for their Valid Use in Overlayer/Substrate Experiments," Surf. Interface Anal. **25**(6), 430–446 (1997).
[52] Z. Zhang, and J.T. Yates, "Band Bending in Semiconductors: Chemical and Physical Consequences at Surfaces and Interfaces," Chem. Rev. **112**(10), 5520–5551 (2012).
[53] N. Taoka, W. Mizubayashi, Y. Morita, S. Migita, H. Ota, and S. Takagi, "Nature of interface traps in Ge metal-insulator-semiconductor structures with GeO_2 interfacial layers," J. Appl. Phys. **109**(8), 084508 (2011).
[54] H.-C. Chang, S.-C. Lu, T.-P. Chou, C.-M. Lin, and C.W. Liu, "First-principles study of Ge dangling bonds with different oxygen backbonds at Ge/GeO_2 interface," J. Appl. Phys. **111**(7), 076105 (2012).
[55] M. Houssa, G. Pourtois, E. Scalise, V. Afanas'ev, and A. Stesmans, "Theoretical Study of Ge Dangling Bonds in GeO_2 and Correlation with ESR Results at Ge/GeO_2 Interfaces," ECS Trans. **41**(3), 39–45 (2011).
[56] T.U. Kampen, and W. Mönch, "Lead contacts on Si(111):H-1 × 1 surfaces," Surf. Sci. **331–333**, 490–495 (1995).
[57] R.A. Razera, A. Moehlecke, and I. Zanesco, "Minority Carrier Lifetime Estimation by Photoconductance Decay for Silicon Wafers Immersed in HF," IEEE J. Photovolt. **7**(4), 1004–1008 (2017).
[58] W.P. Bai, N. Lu, J. Liu, A. Ramirez, D.L. Kwong, D. Wristers, A. Ritenour, L. Lee, and D. Antoniadis, in *2003 Symp. VLSI Technol. Dig. Tech. Pap. IEEE Cat No03CH37407* (Japan Soc. Applied Phys, Kyoto, Japan, 2003), pp. 121–122.
[59] R. Zhang, P.C. Huang, N. Taoka, M. Takenaka, and S. Takagi, in *2012 Symp. VLSI Technol. VLSIT* (IEEE, Honolulu, HI, USA, 2012), pp. 161–162.
[60] R. Xie, M. Yu, M.Y. Lai, L. Chan, and C. Zhu, "High-k gate stack on germanium substrate with fluorine incorporation," Appl. Phys. Lett. **92**(16), 163505 (2008).